Strong energy-transfer-induced enhancement of Er3+ luminescence in In2O3 nanocrystal codoped silica films

Tao Lin, Xiaowei Zhang, Jun Xu, Xin Liu, Mark T. Swihart et al.

Citation: Appl. Phys. Lett. **103**, 181906 (2013); doi: 10.1063/1.4827883
View online: http://dx.doi.org/10.1063/1.4827883
View Table of Contents: http://apl.aip.org/resource/1/APPLAB/v103/i18
Published by the AIP Publishing LLC.

Strong energy-transfer-induced enhancement of Er^{3+} luminescence in In_2O_3 nanocrystal codoped silica films

Tao Lin,[1,2] Xiaowei Zhang,[1] Jun Xu,[1,a)] Xin Liu,[2] Mark T. Swihart,[2] Ling Xu,[1] and Kunji Chen[1]

[1]*National Laboratory of Solid State Microstructures, School of Electronic Science and Engineering and School of Physics, Nanjing University, Nanjing 210093, China*

[2]*Department of Chemical and Biological Engineering, University at Buffalo (SUNY), Buffalo, New York 14260, USA*

(Received 11 September 2013; accepted 16 October 2013; published online 29 October 2013)

Co-doping of sol-gel processed SiO_2 thin films with Er^{3+} ions and In_2O_3 nanocrystals produced a 100-fold enhancement of Er^{3+}-related 1.54 μm emission compared to films doped only with Er^{3+}. Quantitative studies of temperature-dependent photoluminescence spectra show that this dopant-concentration-dependent luminescence enhancement is a result of energy transfer from In_2O_3 to Er^{3+} ions. The dominant nonradiative recombination for Er^{3+} is energy transfer to hydroxyl groups, which is suppressed by proper thermal treatment. These results demonstrate that In_2O_3 nanocrystals have high potential for use as a sensitizer of Er^{3+} ions in high-performance fiber amplifiers. © *2013 AIP Publishing LLC*. [http://dx.doi.org/10.1063/1.4827883]

Erbium (Er) ion doped silica materials have attracted widespread attention based on their potential applications in optical amplifiers for fiber communications and silicon photonics.[1] Er^{3+} ions exhibit a sharp emission line at 1.54 μm, which corresponds to the minimum loss band of silica based optical fibers. Doping with fluorescent rare earth ions also provides a path to realize Si-based light emitters, which are essential to monolithic integration. Unfortunately, the small excitation cross-section of Er^{3+} ions in a SiO_2 matrix leads to insufficient emission efficiencies of these materials. A proven effective strategy to overcome this problem is co-doping with semiconductor nanocrystals (NCs), such as silicon,[2] zinc oxide (ZnO),[3] or tin oxide (SnO_2).[4] This approach relies on the ability of the NCs to transfer energy to nearby Er^{3+} ions. These co-doped NCs have relatively large absorption cross-sections for incident light of appropriate wavelength, due to their efficient band-to-band transitions. The optimal absorbed photon energy depends upon the NC band-gap energy, which is tunable by adjusting NC size in the quantum confinement regime. The absorbed energy is transferred to nearby Er^{3+} ions through Förster resonance energy transfer (FRET), enhancing the infrared Er^{3+}-related emission.

In this work, silica films co-doped with Er^{3+} ions and indium oxide (In_2O_3) NCs were fabricated by a sol-gel approach and subsequent thermal treatment.[5] Sol-gel processing introduces several advantages in fabrication of rare-earth (RE) doped silica films, including a high degree of homogeneity of the formed SiO_2 matrix, uniform distribution of dopants, precise control of the dopant concentrations, and relatively low fabrication temperature compared to traditional melting processes. In_2O_3 NCs were selected as a sensitizer for Er^{3+} ions for the following reasons: (1) In_2O_3 is a wide-band-gap semiconductor with a direct band-gap of 3.6 eV.[6] The mismatch between Er^{3+} excited state ($^4F_{13/2}$) and In_2O_3 band-gap provides a huge barrier to reverse energy transfer from Er^{3+} ions to In_2O_3 NCs. Such reverse energy transfer is commonly observed in the silicon-Er^{3+} co-doped system.[7] (2) The modest crystallization temperature of In_2O_3 is compatible with the post-annealing process required to form a compact silica matrix. Sol-gel-processed silica films contain a high concentration of hydroxyl groups, which are detrimental to Er^{3+} emission.[8] Post-annealing treatment at 850 to 950 °C is an effective way to reduce the hydroxyl content. We have shown in previous work that a high concentration of separate In_2O_3 NCs is formed in this temperature range, without the production of substantial amounts of In-Si-O alloy phases.[9] (3) The spectral overlap between In_2O_3 surface-defect-related emission and Er^{3+} characteristic absorption is expected to allow efficient energy transfer. Here, we show that FRET from In_2O_3 NCs to Er^{3+} ions dramatically enhances the Er^{3+} emission, and we quantitatively evaluate the energy transfer efficiency by systematic temperature-dependent photoluminescence (PL) measurements.

A mixture of tetraethyl orthosilicate (TEOS), ethanol (EtOH), and deionized water (volume ratio = 1:6:3) was used to form a silica sol. Indium nitrate ($In(NO_3)_3$) and erbium nitrate ($Er(NO_3)_3$) salts were added as precursors of In_2O_3 NCs and Er^{3+} ions, respectively. These precursors were selected for their high solubility in the aqueous sol. The transparent solution was hydrolyzed by adding HCl and heating to 65 °C. The resulting wet gel was spin-coated onto clean intrinsic silicon substrates then dehydrated at 400 °C to form a compact amorphous silica film. The films were further annealed at up to 1000 °C in air to reduce the concentration of residual hydroxyl groups. Crystalline In_2O_3 clusters formed and grew *in situ* during the post-anneal process by decomposition of $In(NO_3)_3$.

Fig. 1(a) shows a transmission electron microscopy (TEM) image of a sample that is co-doped with In_2O_3 NCs and Er^{3+} ions. Here, the concentration of indium is 20 mol. % in SiO_2 and the concentration of erbium is 2 mol. %. This sample is labeled as "sample $78SiO_2$-20In:2Er," and this

a)Author to whom correspondence should be addressed. Electronic mail: junxu@nju.edu.cn

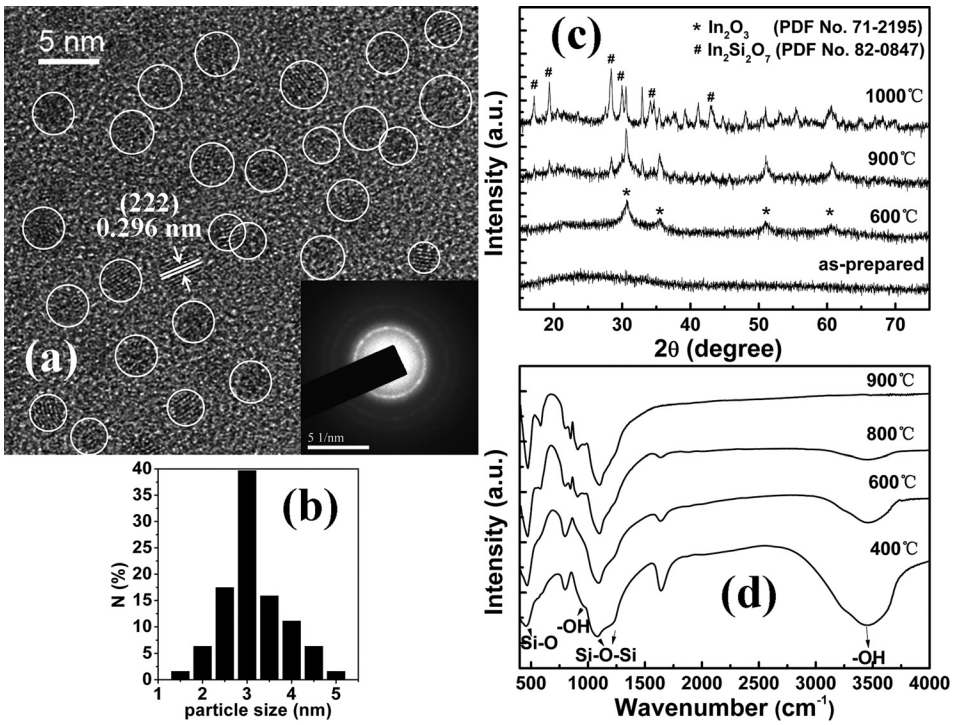

FIG. 1. (a) TEM image of the $78SiO_2$-20In:2Er sample annealed at 900 °C. Inset is the selected area electron diffraction pattern. (b) Size distribution of In_2O_3 NCs in $78SiO_2$-20In:2Er sample. (c) XRD patterns of $78SiO_2$-20In:2Er sample after annealed at different temperatures. (d) FTIR spectra of $78SiO_2$-20In:2Er sample annealed at different temperatures.

naming convention is used throughout the remainder of the manuscript. After annealed at 900 °C for 2 h, spherical crystalline clusters with an average size of 3 nm in diameter can be seen discretely embedded in the amorphous silica matrix. Fig. 1(b) demonstrates their size distribution. X-ray diffraction (XRD) was used to further determine microstructures of the $78SiO_2$-20In:2Er sample, as shown in Fig. 1(c). The patterns for films annealed at 600 to 900 °C exhibit peaks that can be assigned to cubic phase In_2O_3 crystals. Increasing the annealing temperature resulted in narrowing of these peaks, which reflects growth of the NCs. The XRD pattern from the sample annealed at 1000 °C shows the presence of another phase corresponding to a Si-In-O compound, indicating the deterioration of individual In_2O_3 NC structures. The decrease in residual hydroxyl group concentration in the silica matrix after annealing was assessed by Fourier transform infrared (FTIR) spectroscopy (Fig. 1(d)). The broad –OH stretching band centered at 3500 cm^{-1} diminishes in relative intensity with increasing annealing temperature and is absent after annealing at 900 °C.

Fig. 2(a) is the room temperature PL spectrum of the $78SiO_2$-20In:2Er sample after annealing at 900 °C. As seen in the bottom curve, several discrete emission peaks related to Er^{3+} ions are excited by 315 nm UV light. The emission at 525 nm, 547–560 nm, 653–670 nm, and 980 nm correspond to the transitions from $^2H_{11/2}$, $^4S_{3/2}$, $^4F_{9/2}$, and $^4I_{11/2}$ state to $^4I_{15/2}$ ground state, respectively. The much stronger infrared peak at 1540 nm arises from $^4I_{13/2} \rightarrow {}^4I_{15/2}$ transition of Er^{3+} ions. A broader visible emission band centered at 610 nm, ascribable to In_2O_3 defect states like oxygen vacancies, which are commonly found at metal oxide NC surfaces,[10] is also observed. Photoluminescence excitation (PLE) spectra were measured to trace the origin of both Er^{3+}-related emission and In_2O_3-related emission. The PLE spectrum for 1540 nm emission exhibits four sharp peaks at 382 nm, 490 nm, 525 nm, and 658 nm which correspond to the transitions from $^4I_{15/2}$ ground state of Er^{3+} to $^5G_{11/2}$, $^4F_{7/2}$, $^2H_{11/2}$, and $^4F_{9/2}$ state, respectively. The PLE spectra for both 610 nm emission and 1540 nm emission show a strong excitation peak at 315 nm. In our previous work, similar excitation peaks were found in samples co-doped with In_2O_3 and other rare earth ions like Eu^{3+}. In those cases, the peaks blue-shifted with decreasing In_2O_3 NC sizes.[9] So we ascribe them to the band-to-band transition in In_2O_3 NCs whose band-gaps are enlarged by quantum confinement. The inset shows the annealing temperature dependence of these PL intensities. The intensity of 1540 nm Er^{3+}-related emission increases with increasing annealing temperature, and reaches its maximum for annealing at 900 °C. This increased intensity is attributed to elimination of hydroxyl groups and increased crystallinity of In_2O_3 NCs, as shown by the XRD patterns and FTIR spectra in Fig. 1. The decline after 900 °C is ascribed to the appearance of the Si-In-O phase, indicating that 900 °C is the optimal annealing temperature for the In_2O_3-doped silica films. All the samples discussed below were annealed at 900 °C, unless explicitly stated otherwise. The intensity of 610 nm emission demonstrates a similar enhancement but was maximized at 800 °C. The 610 nm In_2O_3-related emission is not only quenched by –OH groups but also by FRET to surrounding Er^{3+} ions, which becomes more efficient with increasing annealing temperature. Consequently, we believe that in going from 800 to 900 °C annealing temperature, increased FRET to Er^{3+} dominates the effects of decreased –OH concentration and increased In_2O_3 crystallinity.

Fig. 2(b) shows the dependence of PL intensity on dopant concentrations. The introduction of In_2O_3 NCs enhances 1540 nm Er^{3+}-related emission, as the PL intensity increases with increasing indium concentration from 0 mol. % to 20 mol. % at a fixed Er^{3+} concentration of 2 mol. %. Compared to the indium-free sample (excited at 382 nm), the PL intensity of the 20 mol. % indium sample was enhanced

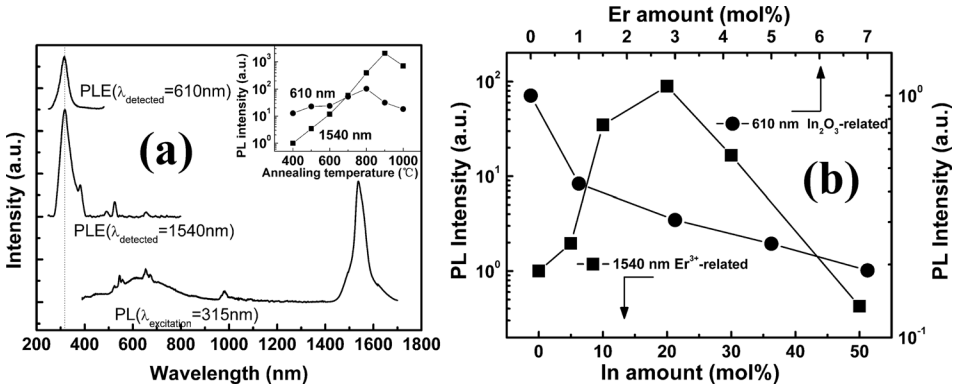

FIG. 2. (a) PL spectrum (bottom line) of $78SiO_2$-20In:2Er sample annealed at 900 °C, excited by 315 nm xenon lamp and corresponding PLE spectra (top and middle line). The top line shows PLE for the 610 nm emission, originating from In_2O_3 surface defects, while the middle line shows PLE for the 1540 nm emission assigned to the Er^{3+} $^4I_{13/2}$-$^4I_{15/2}$ transition. The inset shows the annealing temperature dependence of both PL intensities. (b) Dependence of 1540 nm Er^{3+}-related PL intensity (full square, Er amount = 2 mol. %) on In content and dependence of 610 nm In_2O_3-related PL intensity (full circle, In amount = 20 mol. %) on Er content. All samples were excited by 315 nm light from a Xenon lamp except the indium-free sample which was excited at 382 nm according to the characteristic absorption of Er^{3+} ions.

by two orders of magnitude after correcting all PL intensities by excitation power. Increasing the indium concentration beyond 20% resulted in aggregation and formation of larger In_2O_3 particles. This, in turn, produced a decline of FRET efficiency and Er^{3+}-related PL intensity. On the other hand, as shown in the full circle plots, the introduction of Er^{3+} ions weakens the 610 nm In_2O_3-related emission, as the PL intensity decreases monotonically with increasing erbium concentration. These results demonstrate the concentration-dependent energy transfer from In_2O_3 NCs to Er^{3+} ions in the amorphous SiO_2 matrix.

Based on the PL and PLE observations, we believe that, along with direct excitation, Er^{3+} ions can be excited by FRET from nearby In_2O_3 NCs. This diminishes the visible emission originating from recombination in In_2O_3 surface defect states. The Er^{3+} ions lose part of their excited energy in several nonradiative transitions and finally emit 1540 nm infrared photons via the $^4I_{13/2} \rightarrow {}^4I_{15/2}$ transition. The spectral overlap between the 610 nm emission band related to In_2O_3 NC surface defects and the characteristic excitation peaks of Er^{3+} ions in the visible range is a precondition for efficient FRET.

We measured the temperature dependences of PL intensities to further investigate and better quantify the interactions between the Er^{3+} ions and In_2O_3 NCs. Steady-state PL measurements were performed over a temperature range from 10 to 300 K. PL was excited by a 325 nm He-Cd laser. Plots of integrated PL intensities for the broad In_2O_3-related emission of samples containing either only In_2O_3 NCs or both In_2O_3 NCs and Er^{3+} ions (plot S1 and plot S2, respectively) are shown in Fig. 3. They are both found to decrease strongly with increasing temperature from 60 to 300 K. This thermally activated PL quenching is attributed to phonon-assisted nonradiative recombination. In this model, the observed PL intensities should follow the following modified Arrhenius equation:[11]

$$\frac{I_{VIS}(T)}{I_{VIS0}} = \frac{1}{1 + \frac{k_{nr\infty}}{k_r}\exp\left(-\frac{E_{act}}{kT}\right)}, \quad (1)$$

where I_{VIS0} is the low temperature intensity, $k_{nr\infty}$ and k_r are the decay rate of dominant nonradiative recombination at $T \rightarrow \infty$ and the decay rate of radiative recombination, which are temperature-independent, E_{act} is the activation energy of the nonradiative recombination process, and k is Bolzmann's constant.

As shown in the inset, the plots of $(I_{VIS0}/I_{VIS} - 1)$ vs. $1/T$ for In_2O_3-related PL intensity, with and without erbium, produced straight lines. This implies that the proposed model describes the experimental phenomenon quite well in the range of 60–300 K. The activation energy values derived from slopes are $E_{act} \sim 44$ meV for the Er^{3+}-free sample and $E'_{act} \sim 46$ meV for the $In_2O_3 + Er^{3+}$ sample. These similar activation energy values indicate that the samples with and without Er^{3+} have the same dominant nonradiative recombination pathways in In_2O_3 particles. This activation energy represents the average energy necessary to dissociate a

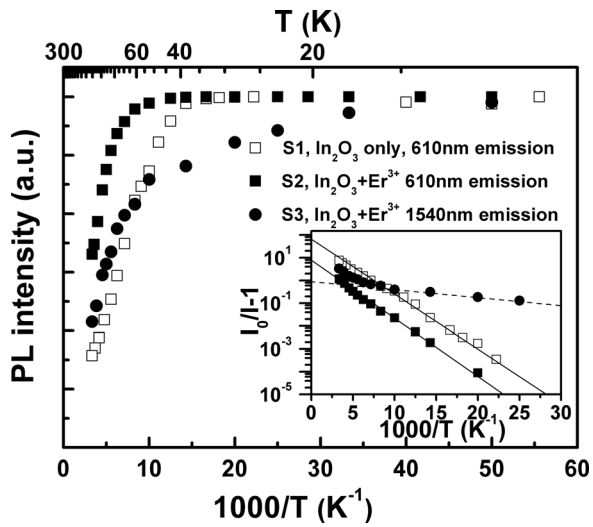

FIG. 3. Temperature-dependence of the PL intensities. Plots S1, S2, and S3 represent visible In_2O_3-related PL intensities of sample $80SiO_2$-20In, visible In_2O_3-related PL intensities of sample $78SiO_2$-20In:2Er, infrared Er^{3+}-related PL intensities of sample $78SiO_2$-20In:2Er, respectively. The inset illustrates the $(I_0/I-1)$ vs. T^{-1} plots that are used to guide the Arrhenius fitting. Two solid lines are the fitting for S1 and S2. The dashed line is the fitting for the modified plot S3/S2 from S3.

bound exciton in surface defect levels and is expected to be close to the localized exciton binding energy of In_2O_3. The prefactors derived from intercepts are as $k_{nr\infty}/k_r \sim 50$ and $(k_{nr\infty}/k_r)' \sim 4$, respectively. Here, based on the model of FRET to Er^{3+} ions, if we define the energy transfer rate as k_{ET}, the prefactor for $In_2O_3 + Er^{3+}$ sample can be given by $(k_{nr\infty}/k_r)' = k_{nr\infty}/(k_r + k_{ET})$, which explains the decline of this prefactor.

The thermal luminescence quenching of infrared Er^{3+}-related emission of the $In_2O_3 + Er^{3+}$ sample (plot S3 in Fig. 3) was also treated using the same model. However, the modified Arrhenius equation does not fit the plots well (full circles in Fig. 3 and the inset). Unlike the In_2O_3 NCs which are excited directly by the pump laser, the Er^{3+} ions are mostly excited through energy transfer from In_2O_3 NCs. This excitation efficiency is proportional to energy transfer efficiency $\eta_{ET}(T)$, which is also proportional to $I_{VIS}(T)$ of the In_2O_3-related emission of the same $In_2O_3 + Er^{3+}$ sample. Taking this into account, we find the following behavior for the Er^{3+}-related PL intensity:

$$\left(\frac{I_{IR}(T)}{I_{IR0}}\right)' = \frac{1}{1 + W\exp\left(-\frac{E_{actIR}}{kT}\right)} \times \left(\frac{I_{VIS}(T)}{I_{VIS0}}\right)', \quad (2)$$

in which the second term $(I_{VIS}(T)/I_{VIS0})'$ has already been measured in this work (plot S2 in Fig. 3). By fitting the S2 plots with Eq. (2), we obtained an activation energy of $E_{actIR} \sim 10\,\text{meV}$. This fit is shown as the dashed fitting line in the inset. Various nonradiative recombination pathways are available to excited Er^{3+} ions, including reverse energy transfer to NCs, energy transfer to nearby Er^{3+} ions through cross relaxation and energy loss to the host matrix through phonon emission. Here, the possibility of reverse energy transfer to In_2O_3 NCs is extremely small, due to the huge mismatch between energies of the Er^{3+} excited state ($^4F_{13/2}$) and In_2O_3 band-gap. Moreover, concentration quenching effects were not observed in samples with erbium concentration up to 5 mol. %. Based on the result that the PL intensity is strongly determined by the concentration of residual hydroxyl groups, we conclude that the excited Er^{3+} ions transfer energy to the vibrations of hydroxyl groups and the dominant nonradiative recombination pathway in this system is energy transfer to the host material. Because just two vibrations of hydroxyl groups are sufficient to bridge the $^4I_{13/2} \rightarrow {}^4I_{15/2}$ transition of about $6500\,\text{cm}^{-1}$, the obtained activation energy may be explained as the average energy mismatch between two hydroxyl group vibrations and the $^4I_{13/2} \rightarrow {}^4I_{15/2}$ transition.[8]

In summary, amorphous SiO_2 films uniformly co-doped with In_2O_3 NCs and Er^{3+} ions have been fabricated by a sol-gel method. The infrared PL at 1540 nm, related to Er^{3+} $^4I_{13/2} \rightarrow {}^4I_{15/2}$ transition, is 100 times larger than in the indium-free sample. The dependences of Er^{3+}-related PL intensity on In_2O_3 concentration and of In_2O_3-related PL on Er^{3+} concentration indicate energy transfer from In_2O_3 NCs to Er^{3+} ions. The proposed FRET process is supported by temperature-dependent PL measurements, for it demonstrated an In_2O_3-PL-related thermal quenching process of Er^{3+} PL intensity. The dominant nonradiative recombination pathway for excited Er^{3+} ions is suggested to be energy transfer to vibrational modes of hydroxyl groups in the SiO_2 matrix. Post-annealing at 900 °C reduces the concentration of hydroxyl groups, and correspondingly reduces non-radiative recombination.

This work was supported by "973" program (No. 2013CB632101), NSFC (Nos. 61036001 and 11274155), and PAPD. The authors also thank SSSAP by China Scholarship Council 2011.

[1]D. Liang and J. E. Bowers, Nat. Photonics **4**(8), 511 (2010).
[2]I. Izeddin, D. Timmerman, T. Gregorkiewicz, A. S. Moskalenko, A. A. Prokofiev, I. N. Yassievich, and M. Fujii, Phys. Rev. B **78**(3), 035327 (2008); O. Savchyn, R. M. Todi, K. R. Coffey, and P. G. Kik, Appl. Phys. Lett. **94**, 241115 (2009).
[3]F. Xiao, R. Chen, Y. Q. Shen, Z. L. Dong, H. H. Wang, Q. Y. Zhang, and H. D. Sun, J. Phys. Chem. C **116**(24), 13458 (2012).
[4]J. del-Castillo, V. D. Rodríguez, A. C. Yanes, and J. Méndez-Ramos, J. Nanopart. Res. **10**(3), 499 (2008); S. Brovelli, N. Chiodini, F. Meinardi, A. Monguzzi, A. Lauria, R. Lorenzi, B. Vodopivec, M. C. Mozzati, and A. Paleari, Phys. Rev. B **79**(15), 153108 (2009).
[5]N. Wan, J. Xu, T. Lin, X. G. Zhang, and L. Xu, Appl. Phys. Lett. **92**(20), 201109 (2008).
[6]P. Erhart, A. Klein, R. G. Egdell, and K. Albe, Phys. Rev. B **75**(15), 153205 (2007).
[7]A. Pitanti, D. Navarro-Urrios, N. Prtljaga, N. Daldosso, F. Gourbilleau, R. Rizk, B. Garrido, and L. Pavesi, J. Appl. Phys. **108**(5), 053518 (2010).
[8]M. Fukushima, N. Managaki, M. Fujii, H. Yanagi, and S. Hayashi, J. Appl. Phys. **98**(2), 024316 (2005).
[9]T. Lin, X. Ding, J. Xu, N. Wan, L. Xu, and K. Chen, J. Appl. Phys. **109**, 083512 (2011).
[10]Y. Yu, D. Chen, Y. Wang, P. Huang, F. Weng, and M. Niu, Phys. Chem. Chem. Phys. **11**(39), 8774 (2009); O. L. Stroyuk, V. M. Dzhagan, V. V. Shvalagin, and S. Y. Kuchmiy, J. Phys. Chem. C **114**(1), 220 (2010); X. Liu and M. T. Swihart, Nanoscale **5**(17), 8029 (2013).
[11]R. W. Collins and W. Paul, Phys. Rev. B **25**(8), 5257 (1982).